

Assessing the accuracy of ocean tide models by using variance of residuals of satellite sea level heights in the Patagonian shelf

MARÍA FLORENCIA DE AZKUE¹, ENRIQUE EDUARDO D'ONOFRIO², ALAN JACOBS³

¹ <https://orcid.org/0000-0002-2331-4745>

² <https://orcid.org/0000-0003-0432-5235>

³ <https://orcid.org/0000-0002-7336-0715>

OPEN ACCESS

Received:

02/11/2022

Revised :

21/11/2022

Accepted:

30/11/2022

Published online:

30/12/2022

Editor Asociado:

Dr. Julio Salcedo Castro

ISSN 0718-686X

ABSTRACT

This work proposes to compare the astronomical tidal predictions obtained by using the totality of the constituents provided by seven global tide models and by the Center for Topographic studies of the Ocean and Hydrosphere (CTOH). To quantify this comparison, the variance of residuals of satellite sea level heights are computed from 1992 to 2019, for each model and CTOH. As a case study, we focus on the Patagonian shelf. It is found that the most accurate tidal predictions are obtained when using FES2014 model and CTOH harmonic constants. It is also observed that the decrease in variance values is due to the addition of certain minor constituents. As an example, in the case of CTOH, a location yields a reduction of more than 57% in the variance values when 9 minor constituents are added to the nine common ones. Likewise, in the case of FES2014, variance reduction over this same location is more than 56% by incorporating 14 minor constituents. Finally, a comparison of the amplitudes and phases values of the common constituents among models and the CTOH shows that these values are practically the same. However, when comparing predictions, very dissimilar results are obtained among models.

Keywords: global tide models, tide predictions, residuals of sea level heights.



Estudio de la precisión de modelos de marea mediante la varianza de los residuos de alturas satelitales en la plataforma patagónica

Author contributions:

F.M.: conceptualization, investigation, methodology, software, writing, original draft, review & editing

D'O.E.E.: conceptualization, investigation, methodology, software, review & editing

J.A.: writing-review & editing

Conflict of interest:

No existen conflictos de intereses

Funding:

Proyecto PIDDEF 10/20: Modelo de marea astronómica de alta resolución para el litoral marítimo bonaerense y su plataforma continental, a partir de observaciones de marea, información satelital y resultados de modelación numérica"

Proyecto B-ESCM-0010/20: Cálculo de la distancia entre los planos de reducción de sondajes y el elipsoide WGS84 para el sector comprendido entre los paralelos 33°S y 59°S y los meridianos 69°50'W y 52°30'W

RESUMEN

Este trabajo propone comparar las predicciones de mareas astronómicas obtenidas utilizando la totalidad de las componentes proporcionadas por siete modelos globales de mareas y por el Centro de Estudios Topográficos del Océano y la Hidrosfera (CTOH). Para cuantificar esta comparación, se calcula la varianza de los residuos de las alturas satelitales del nivel del mar desde 1992 hasta 2019, para cada modelo y el CTOH. Como caso de estudio nos centramos en la plataforma continental patagónica. Se encuentra que las predicciones de marea más precisas se obtienen cuando se utiliza el modelo FES2014 y las constantes armónicas del CTOH. También se observa que la disminución de los valores de la varianza se debe a la adición de ciertas componentes menores. Como ejemplo, en el caso de CTOH, en una localización se registra una reducción de más del 57% en los valores de varianza cuando se añaden 9 componentes menores a las 9 comunes. Asimismo, en el caso del FES2014, la reducción de la varianza en esta misma localización es superior al 56% al incorporar 14 componentes menores. Finalmente, la comparación de los valores de amplitudes y fases de las componentes comunes entre los modelos y el CTOH muestra que estos valores son prácticamente iguales. Sin embargo, al comparar las predicciones, se obtienen resultados muy disímiles entre los modelos.

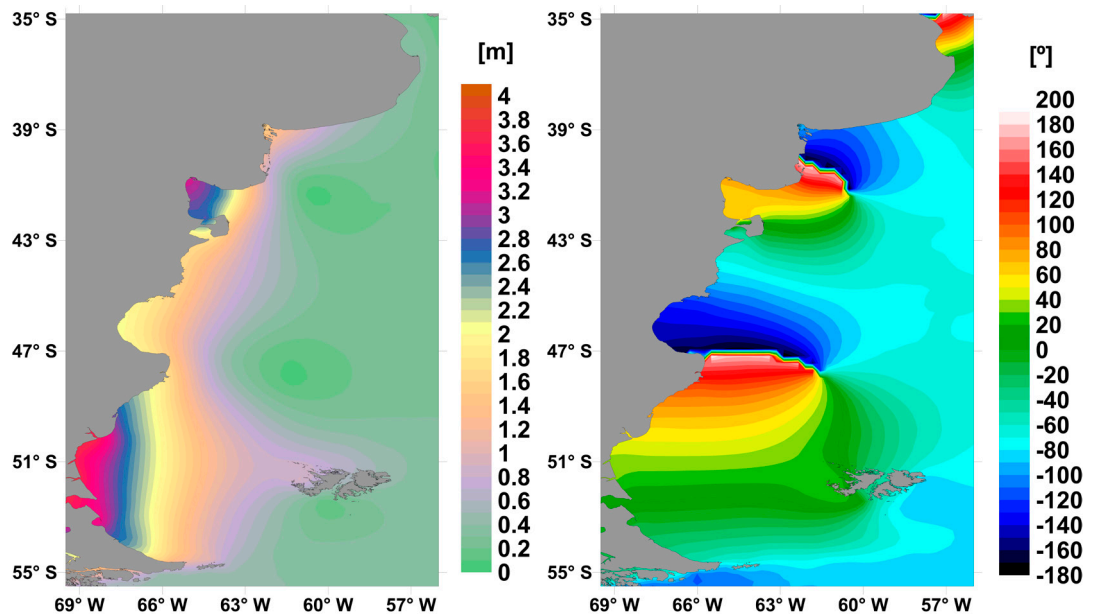
Palabras clave: modelos globales de marea, predicciones de marea, componentes menores.

INTRODUCTION

Astronomical ocean tide has a large impact on the coastal population, offshore applications, environmental observations, and exploration. Tides are the principal contributor to the disposal and movement of sediments, tracers, and pollutants (e.g. Lee, 2004; Pugh & Woodworth, 2014). Astronomical tide can modify physical and dynamical processes, and be the main forcing of the surface circulation (Palma 2018). Thus, several showed that astronomical tide might affect surface geostrophic circulation, potential and eddy kinetic energy distributions, surface temperatures, mixing layer, and net heat flows (e.g. Bhagawati 2018, Egbert & Ray, 2001; Kang, 2012). In addition, in the open-ocean, tidal dissipation may influence the large-scale circulation and vertical mixing (Egbert & Ray, 2001; Green 2009; Wunsch & Ferrari, 2004;). Furthermore, tidal height is one of the most important geophysical adjustments applied to altimeter data (e.g. Carrère 2016; Desportes 2007). All the above-mentioned inferences from the tide make its accurate knowledge and prediction being essential. The availability of sea surface height (SSH) global data, provided by satellite altimetry, has triggered global and regional ocean tide numerical model developments. In addition to the aspects already listed, tide models are key to determining surface topography, the gravity field, and depth datum models with high accuracy (de Azkue 2021). Furthermore, the errors from tide models pose limitations not only for determining the temporal gravity field but also for estimating mass transport processes (Koop & Rummel, 2007; Pail 2016). Although the number and combination of constituents to obtain better tide predictions might depend on the region considered, some of the efforts to improve tide models are directed toward incorporating minor tidal constituents (Hart-Davis 2021a). These constituents become increasingly important, especially in the coastal and shelf regions. In particular, the amplitude of the constituents depends on the location and the interactions of resonant modes over the region. In that sense, the southwest Atlantic continental shelf, also known as the Patagonian shelf (PS), presents tidal ranges that can exceed 10 m (D'Onofrio 2016) being among the largest in the global ocean.

When it is required to detiding observational data, or set boundary conditions, it is usually needed to take the available tide models into consideration and compare them to choose the one that best fits the area under study. This is particularly important when it comes to global models, as their performance may vary from region to region. For example, intermodel discrepancies appear to be substantially elevated in shelf regions relative to the open ocean (Stammer 2014). Thus, astronomical tide model comparison is usually performed through Root Mean Square (RMS) and Root Sum Square (RSS) between the harmonic constants of a model and in-situ tidal harmonic constants (e.g. Hart-Davis 2021a; Oreiro 2014; Stammer 2014). However, this methodology may involve two limitations. The first one refers to the impossibility of having a set of harmonic constants in situ. It limits the comparison data to those for which long time series are available for computing accurate harmonic constants (Zaron & Elipot, 2021; Hart-Davis 2021a). That occurs in large areas in the open sea or in inshore regions with a few or no tide gauges. In this sense, the Southwest Atlantic Ocean is a region with very few observations recorded by tide gauges (Holgate 2013). The second limitation of the RMS method is the constraint of considering only the common constituents among models to be compared (generally the major ones). The latter implies that, for a given model, only a percentage of the provided tidal constituents is assessed, mainly in the coastal and shelf regions, where minor constituents appear to be more significant. In addition, the major constituents tend to have similar harmonic constant values between models, as they represent the main contributors to the astronomical forcing, representing a difficulty

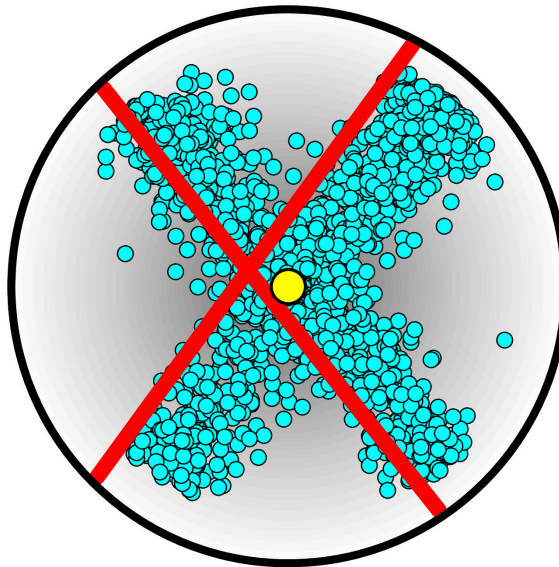
Fig. 1.
Amplitudes (left) and
cotidal charts
(right) of the main
semidiurnal
tidal constituent (M_2)
over the study domain
(de Azkue, 2017).



to choose the most appropriate model. Thus, the RMS method does neither allow comparing all constituents nor their contribution to sea level height. To overcome these limitations, comparing the astronomical tide predictions obtained by using the totality of the constituents provided by seven global tide models (DTU10, EOT20, GOT410c, FES2014, TPXO9v1, TPXO9v2, TPXO9v5) and by the Center for Topographic studies of the Ocean and Hydrosphere (CTOH) is being proposed. To quantify the comparison of tide predictions series from models and CTOH, the variance of residuals of satellite sea level heights are computed from 1992 to 2019. Variance reduction tests on altimetry sea level anomalies constitute a standard method for evaluating ocean tide models (Hart-Davis 2021a; Stammer 2014).

As a case study, we focus on PS due to its particular dynamic and tidal characteristics. The study domain is located in the region between 35°S and 55.5°S latitudes and 56°W and 69.5°W longitudes. There, tidal forcing and strong offshore winds dominate the circulation (Palma 2004). The bathymetry of the PS presents a wide continental shelf with high cliffs at the coast south of 40°S, and the abrupt shelf slope interrupted to the east of the Malvinas Islands by the Malvinas Plateau. The width of the shelf is comparable with a quarter wavelength of a semidiurnal tidal wave, thus resulting in a near-resonant natural system (*e.g.* Middleton & Bode, 1987). This area is also considered as one of the regions of highest energy dissipation by bottom friction (*e.g.* Glorioso, 2000; Moreira, 2011; Palma, 2004; Simionato, 2004). The tidal spectrum is dominated by the principal semidiurnal lunar tide, M_2 , although significant contributions come from several other constituents. The phase of the semidiurnal tidal wave propagates to the north after entering from the south and southeast of the domain, and the largest amplitudes, for M_2 , occur on the mainland coast at 51°S (Fig. 1).

Fig. 2.
Theoretical tracks
are represented
in red, observed
heights (cyan circles)
and barycenter
(yellow circle) of the
observations for the
crossing of tracks
163 and 154.



DATA

Satellite altimeter measurements

The satellite altimeter data used in this work include TOPEX/Poseidon (T/P), Jason1 (J1), Jason2 (J2), and Jason3 (J3) altimetry missions for the period September-1992 to July-2019. As in Stammer (2014) where seven ocean tide models are tested based on remote measurements, the period of satellite observations used in this work partially overlaps with the time span in which global tide models were developed, but not with all of them. For example, all models are independent of the Jason1 geodetic mission data (Stammer 2014). On the other hand, some missions used for the development of the models are not considered for obtaining the satellite heights. This is the example of the assimilated observations by FES2014 model corresponding to the ERS-1, ERS-2, and ENVISAT.

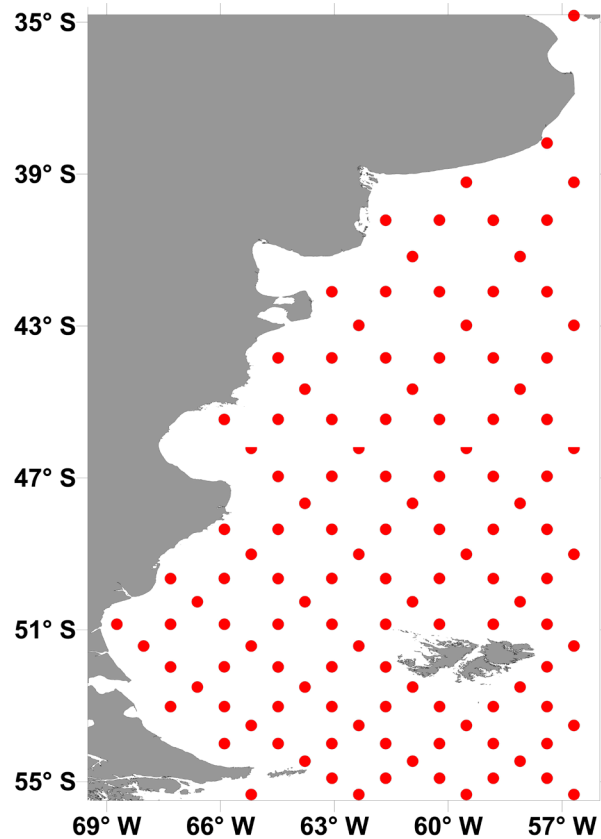
These altimeter products were produced and distributed by AVISO+ (<https://www.aviso.altimetry.fr/>), as part of the SSALTO ground processing segment. We consider the main missions and, in the case of interleaved ones, only when they cross a main mission. Along-track SLA (sea level anomaly) is calculated by AVISO+ following Equation 1.

Equation (1)

$$\begin{aligned}
 SLA = & \textit{altitude} - \textit{range} - \textit{ionospheric correction} - \\
 & \textit{dry tropospheric correction model} - \textit{wet tropospheric correction} - \textit{sea state bias} - \\
 & \textit{solid earth tide} - \textit{ocean tide height} - \textit{pole tide} - \textit{dynamic atmospheric correction} - \\
 & \textit{mean sea surface} - \textit{inter mission bias}
 \end{aligned}$$

In order to obtain a larger number of observations at each site and to achieve results that are more reliable, only the data from the crossovers are taken into account, but not those observations from two interleaved missions. This includes crossovers between two main-tracks and those between a main-track and an interleaved one.

Fig. 3.
Domain crossovers:
the dots correspond
to the 145 locations
of SSht time series
selected in the study
region containing
more than 1000
measurements.



SSht (SLA + ocean tide height) series are calculated by adding astronomical tide correction provided by AVISO+ to the along-track SLA values at each crossover.

Along-track satellite positions may vary by approximately 1 km relative to the nominal track (Chelton 2001). Here we consider all the SSht corresponding to each crossover that are included within a circle of radius 2.5 km, centered in the barycenter that is determined by the positions of the observations of the two ground tracks (Fig. 2).

All SSht comprised within these circles can be considered as observed at their centers. This is justified because the astronomical tide spreads very rapidly, reaching a height variation of less than 1 cm at the edges of the 5 km diameter circle, even in regions with large amplitudes (D'Onofrio 2016). This variation is significantly less than the 2 cm RMS 1D along-track SSH measurement noise (Pujol 2012). Then we selected T/P, J1, J2, and J3 crossovers and computed the SSht series in the barycenters.

An SSht series observation whose value is more than three standard deviations from the mean is considered an outlier and then, only those series containing 1000 or more observations are retained. The objective is to obtain a robust variance of the residuals of sea level heights (VRSL). Thus, 145 locations make up the study domain as shown in Fig. 3.

Tide models and CTOH harmonic constants

To carry out this work we use the gridded harmonic constants from CTOH and from EOT20, DTU10, and GOT4.10c global models. In the case of TPXO9v1, TPXO9v2, TPXO9v5, and FES2014 models, their associated and released software is run. The global models selected here are widely used from state-of-the-art global barotropic tide models.

Finite Element Solution (FES) is an astronomical tide model whose latest version, named FES2014, has been developed in 2014-2016. FES is based on the resolution of the tidal barotropic equations (T-UGO model) in a spectral configuration (Lyard 2006). The accuracy of this solution was improved by assimilating long-term altimetry data (T/P, J1, J2, TPN-J1N, and ERS-1, ERS-2, ENVISAT) and tidal gauges. NOVELTIS, LEGOS, and CLS have produced FES2014 and AVISO+ distributed it, with support from CNES. The model features a new prediction algorithm distributed within the FES2014 package that provides tidal heights at any location of the world ocean. This new prediction code allows the computing of 11 complementary HF constituents by the means of a specific admittance method and about 100 long-period equilibrium ocean waves (<https://www.aviso.altimetry.fr/>).

The latest version in a series of empirical ocean tide (EOT) models developed using residual tidal analysis of multi-mission satellite altimetry at DGFI-TUM, is the EOT20. The model is based on an empirical analysis of seven satellite altimetry missions and four extended missions. The inclusion of more recent altimetry data has improved this latest version of the model compared to the previous one (EOT11a), especially in the coastal regions and over the shelves. The updating tide model focus on improving the coastal estimations of ocean tides by analyzing recent developments in coastal altimetry, particularly the use of the ALES retracker and sea state bias correction (Hart-Davis 2021a)

The model of astronomical ocean tide DTU10 (Technical University of Denmark) has been developed based on FES2004. It has been applied the response method (Munk & Cartwright, 1966) using seventeen years of multimission measurements from T/P, J1, and J2 satellite altimetry for sea level residuals analysis (Yongcun 2010).

The Goddard/Grenoble Ocean Tide (GOT) empirical model, maintained by Richard Ray at NASA- Goddard Space Flight Center, is distributed as a set of tidal harmonic constants (Ray, 1999). The GOT410 is the latest in the series of barotropic tide models. Version "c" takes into account the tidal oscillations of the geocenter, which translates mainly into small changes in the K_1 and O_1 constituents (Desai & Ray, 2014). The model resolution $(1/2)^\circ$ is not appropriate to represent tidal variability on continental shelves or in nearshore regions. On the other hand, it provides good modeling of tides in the deep ocean (Zaron & Elipot, 2021).

TPXO is a series of fully-global models of astronomical ocean tides, which best fits, in a least-squares sense, the Laplace Tidal Equations and altimetry data (Egbert & Erofeeva, 2002). Each new version in a series of TPXO models assimilates more data and also includes an updated bathymetry. Earth and Space Research provides Matlab software, the Tide Model Driver (TMD) package, to access models, output harmonic constants, and make tidal predictions (Erofeeva 2020). Besides the minor constituents $2Q_1$, J_1 , L_2 , M_3 , MU_2 , NU_2 , and OO_1 , included with TPXO9v2/v5a prediction software, other 9 possible inferred constituents are: Σ_1 , Rho_1 , M_1 , Chi_1 , Pi_1 , Phi_1 , $Theta_1$, Λ_2 , T_2 .

Global Models					
Model	Resolution	Constituents			
		Diurnal	Semidiurnal	Short-period	Long-period
GOT4.10c	1/2° x 1/2°	K_1, O_1, P_1, Q_1, S_1	M_2, S_2, N_2, K_2	M_4	
TPX09v1	1/6° x 1/6°			MS_4, MN_4	MM, MF
	1/30° x 1/30°	K_1, O_1, P_1, Q_1, S_1	$M_2, S_2, N_2, K_2, 2N_2$	M_4	
TPX09v2	1/6° x 1/6°	$K_1, O_1, P_1, Q_1, S_1, 2Q_1, J_1, OO_1$	$M_2, S_2, N_2, K_2, 2N_2, L_2, Mu_2, Nu_2$	M_3, M_4, MS_4, MN_4	MM, MF
TPX09v5	1/6° x 1/6°	$K_1, O_1, P_1, Q_1, S_1, 2Q_1, J_1, OO_1$	$M_2, S_2, N_2, K_2, 2N_2, L_2, Mu_2, Nu_2$	M_3, M_4, MS_4, MN_4	MM, MF
FES2014	1/16° x 1/16°	$K_1, O_1, P_1, Q_1, S_1, J_1$	$M_2, S_2, N_2, K_2, 2N_2, E_2, MKS_2, T_2, La_2, R_2, Nu_2, L_2, Mu_2$	$M_3, M_4, MN_4, N_4, MS_4, S_4, M_6, M_8$	SSA, MM, MTM, MF, MSF, MSQM, SA
EOT20	1/8° x 1/8°	$K_1, O_1, P_1, Q_1, S_1, J_1$	$M_2, S_2, N_2, K_2, 2N_2, T_2$	M_4	SA, SSA, MF, MM
DTU10	1/8° x 1/8°	K_1, O_1, P_1, Q_1, S_1	M_2, S_2, N_2, K_2	M_4	
CTOH					
Constituents					
Diurnal	Semidiurnal	Short-period	Long-period		
$2Q_1, Sig_1, Q_1, Ro_1, O_1, MP_1, M_1, K_1, Pi_1, P_1, K_1, Psi_1, Phi_1, Tta_1, J_1, SO_1, OO_1, KQ_1$	$OQ_2, MNS_2, E_2, 2MK_2, 2N_2, Mu_2, N_2, Nu_2, MSK_2, M(SK)_2, M_2, M(KS)_2, MKS_2, La_2, L_2, T_2, S_2, R_2, K_2, MSN_2, KJ_2, 2SM_2$	$2MK_3, M_3, SO_3, MK_3, S_3, SK_3, N_4, 3MS_4, MN_4, M_4, SN_4, MS_4, MK_4, S_4, SK_4, 2MN_6, M_6, MSN_6, 2MS_6, 2MK_6, 2SM_6, MSK_6, 3MS_8$	$SA, SSA, MSM, MM, MSF, MF, MSTM, MTM, MSQM, MQM$		

Table 1. The gridded/estimated constituents and their resolution of the seven astronomical tide models used, and CTOH constituents. The nine common constituents among models are in red.

CTOH offers a set of 73 harmonic constants listed in Table 1 that are called X-TRACK Coastal products (<https://www.aviso.altimetry.fr/en/data/products/sea-surface-height-products/regional/x-tracksla.html>). Tidal constants are estimated from CTOH along-track 1 Hz SLA products (*i.e.* every 6.2 km) and are calculated directly by harmonic analysis of each single time series. The constants used in this work belong to the Atlantic Zone of South America. The improvements of the X-TRACK product and the gain in accuracy of nearshore data are analyzed and described by Birol (2017). The locations of the CTOH constants match the locations of the satellite observations, so it is not necessary to interpolate the values to remove the tide in this case.

Table 1 presents the gridded/estimated constituents and their resolution of the seven astronomical tide models used, and CTOH constituents. The common constituents between the different models are in red. They are $K_1, O_1, P_1, Q_1, M_2, S_2, N_2, K_2$, and M_4 .

METHODOLOGY

The harmonic constants of the EOT20, GOT410c and DTU10 models are obtained by interpolation over the 145 crossovers. To perform this interpolation, different methods are tested: minimum curvature, Kriging, inverse of the weighted distance, modified Shepard, nearest neighbor, radial basis function and triangulation with linear interpolation. The Kriging method is chosen, as it presents the lowest mean squared error of the differences between the harmonic constants obtained for the positions of the crossovers and the corresponding ones for those positions, calculated by interpolation between the values of the grid nodes. The series of tide predictions for each set of constants of the mentioned tide models and CTOH are computed according to Equation 2:

Equation (2)

$$h(t) = \sum_{j=1}^n H_j \cdot f_j \cdot \cos((V + u)_j - g_j)$$

where $h(t)$ is the observed astronomical tide height at t observation time, j is a constituent, n is the number of constituents, H is the amplitude, f is the nodal factor at time t , $(V + u)$ is the equilibrium argument at time t , and g is the modified epoch. In order to maintain the accuracy of the prediction over long periods, the variation of u and f (18.61-year nodal cycle) is considered by calculating them for each t value (Byun & Hart, 2019). The equilibrium arguments and nodal factors are calculated following Cartwright (1985). The predictions are made on dates matching satellite observations in the chosen period (1992-2019).

Time series predictions, at the same mentioned dates, for TPXO9v1, TPXO9v2, TPXO9v5, and FES2014 are obtained by running their associated algorithms (TMD Matlab for TPXO models and `tide_gauge.py` for FES2014). These software predictions allow the inclusion of minor tides and infer some others from a smooth admittance function. Even though it may occur that inference does not provide an accurate estimation of tides (Hart-Davis 2021b). That is found in the case of TPXO9v2 and TPXO9v5 models, in most of the PS. For this reason, predictions are made by calculating constants directly from the models, without inference.

To calculate the residuals of satellite sea level heights, the predictions corresponding to the models and CTOH are subtracted from the 145 SSht series that conform the domain, according to the criteria mentioned in the Data section.

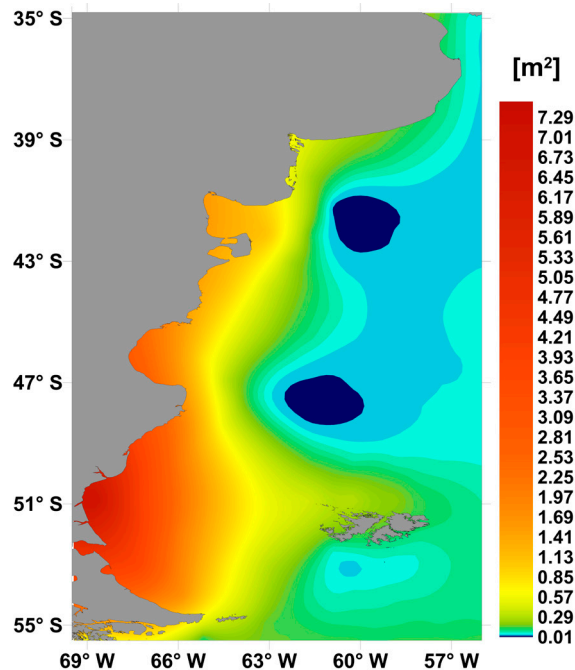
Finally, from the residuals of satellite sea level heights series obtained for each of the seven models and CTOH, the corresponding variance is estimated at each crossover following Equation 3.

EQUATION (3)

$$\text{variance of residuals of sea level heights (VRSL)} = \frac{1}{n} \sum_{t=1}^n (h_t - \bar{h})^2$$

where n is the number of observations of the residual of satellite sea level heights series, h_t is the residual of the satellite sea level height for the t observation and, \bar{h} is the mean of the residual of satellite sea level heights series.

Fig. 4.
Contours of
SSHt variance in
the PS.



RESULTS

Variance of SSHt

Before analyzing the VRSL values, a map of SSHt variances is shown in Fig. 4. SSHt variances obtained at the crossovers are interpolated for better visualization. The PS region is distinguished by its large variability, with variance values of SSHt ranging from 0.2 m^2 and exceeding 7 m^2 . As we mentioned before, this region is characterized by its macro tidal regime, one of the most important in the world (*e.g.* Glorioso & Simpson, 1994; Glorioso & Flather, 1998). In order to appreciate the change in height variability, in the next section, we will exhibit how the values of SSHt variance are modified once the tide is removed using the results of models and CTOH, and then we calculate the corresponding VRSL to assess them.

VRSL comparison

The VRSL obtained at the crossovers after detide SSHt using predictions from models and CTOH are interpolated for better visualization (Fig. 5 A, B, C, D, E, F, G, H). It is observed that for all models the values of variance drop drastically in the PS with respect to Fig. 4 (before the tide has been removed).

The smallest zonal extent delineated by the VRSL values (marked with a white contour on the 0.010 m^2 isoline in Figs. 4A, B, C, D, E, F, G, H) is undoubtedly the one associated with the CTOH (Fig. 5A) and the one corresponding to the FES2014 (Fig. 5D). For the rest of the models, this area is more extensive and records higher VRSLs, especially in the southern part of the region.

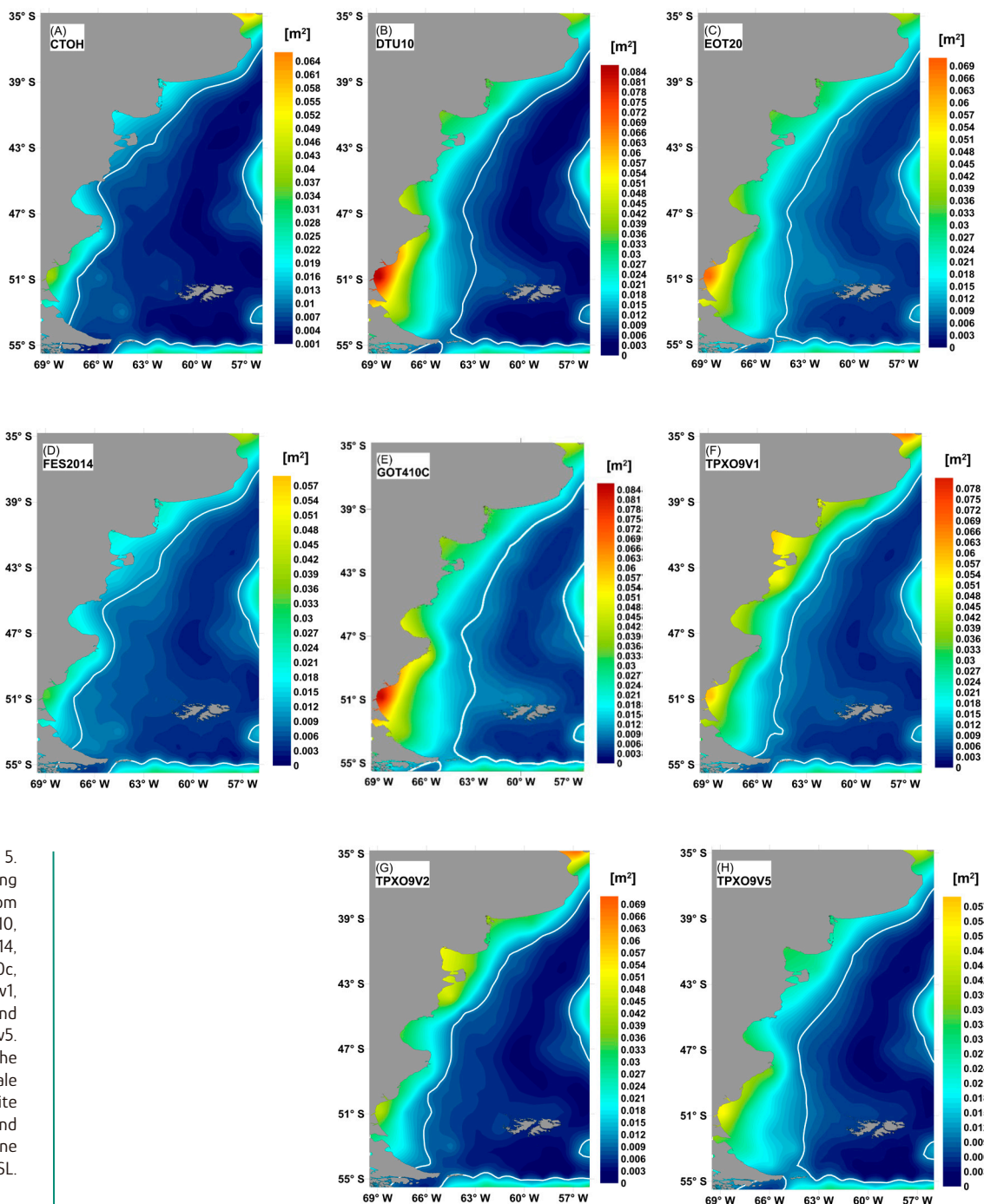


Fig 5.
 VRSL values using
 predictions from
 (A) CTOH, (B) DTU10,
 (C) EOT20, (D) FES2014,
 (E) GOT4.10c,
 (F) TPX09v1,
 (G) TPX09v2, and
 (H) TPX09v5.
 For all the
 maps, the same scale
 color bar is used. White
 contours correspond
 to the 0.010 m^2
 isoline
 of VRSL.

The Río de la Plata estuary also presents discrepancies between models, being the DTU10, EOT20, FES2014, GOT410c, and TPXO9v5 models the ones that showed the best performance.

It is interesting to see the difference between the results of TPXO9 versions (Figs. 5F, G, and H). While TPXO9v5 yields minor VRSL values than the two TPXO9 other versions on the regions of the Río de la Plata estuary, and the area around 38.5°S and 45°S, it shows larger values on south PS than the previous version TPXO9v2. However, the lowest maximum value coincides with that of FES2014 (0.058 m²). The smallest zonal extent of the VRSL region between TPXO9 models is associated with version 2, and the biggest with version 5. Thus, there is no version that enhances the entire domain.

The relatively high VRSL values found in a narrow band in the south of the domain and in the west of it, located outside the PS, match with a part of areas with high variability that are associated with a large mesoscale activity. The Antarctic Circumpolar Current flows over the southern region, while the western region is part of the area of influence of the Zapiola anticyclonic gyre.

Tidal constituents analysis

To analyze wave components we calculate the number of constituents whose amplitudes are larger than or equal to 2 cm for models and CTOH, at each location. The results are displayed in Figs. 6A, B, C, D, E, F, G, and H. The threshold of 2 cm is set considering that constituents with that amplitude values can modify significantly the height of the sea level in areas where tide ranges are in the order of some centimeters. It is observed that the number of constituents increases towards the shore for all models, with maximum values being reached in the south of the shelf. CTOH shows there a crossover with 41 constituents, followed by FES2014 with 21 constituents, EOT20, TPXO9v2, and TPXO9v5 with 15, TPXO9v1 with 12, and DTU10 and GOT410c with 9. Note that this area is where the models yield the largest discrepancies in reducing variance values, and where significance variability in residuals is still observed except for FES2014, CTOH, and TPXO9v2 (Figs. 5A, B, C, D, E, F, G, and H). Quite different is the case for the crossover located outside the continental platform, where the number of tidal constituents with amplitude higher than or equal to 2 cm is no larger than 9 at each location.

In the case of CTOH, a cross-track located in the Río de la Plata estuary displays 48 tidal constituents (Fig. 6A) while the other models do not exceed 9 component waves in the worst-case situation. This large number is mainly explained by the fact that the harmonic analysis methodology used to obtain the harmonic constants by the CTOH allows the recording of variability that corresponds to non-tidal noise. Perturbations of the tidal signal may arise from variations in external forcing like oceanic, meteorological, hydrologic, or climatic and generate a nonstationary tidal response (Matte 2013). Likewise, CTOH shows the same sensibility of adding non-stationary constituents in the part of the two regions that match areas with large mesoscale activity outside the PS that we mentioned above (Fig. 5A, B, C, D, E, F, G, and H). To figure out the impact of decreasing VRSL values by the addition of minor constituents, VRSLs are calculated first by considering only the nine major and common constituents (M_2 , S_2 , N_2 , K_2 , K_1 , O_1 , P_1 , M_4 , Q_1) and then adding the remaining ones sorted by decreasing amplitude, one by one, until the VRSL value becomes stationary. That is until the VRSL reaches a value that does

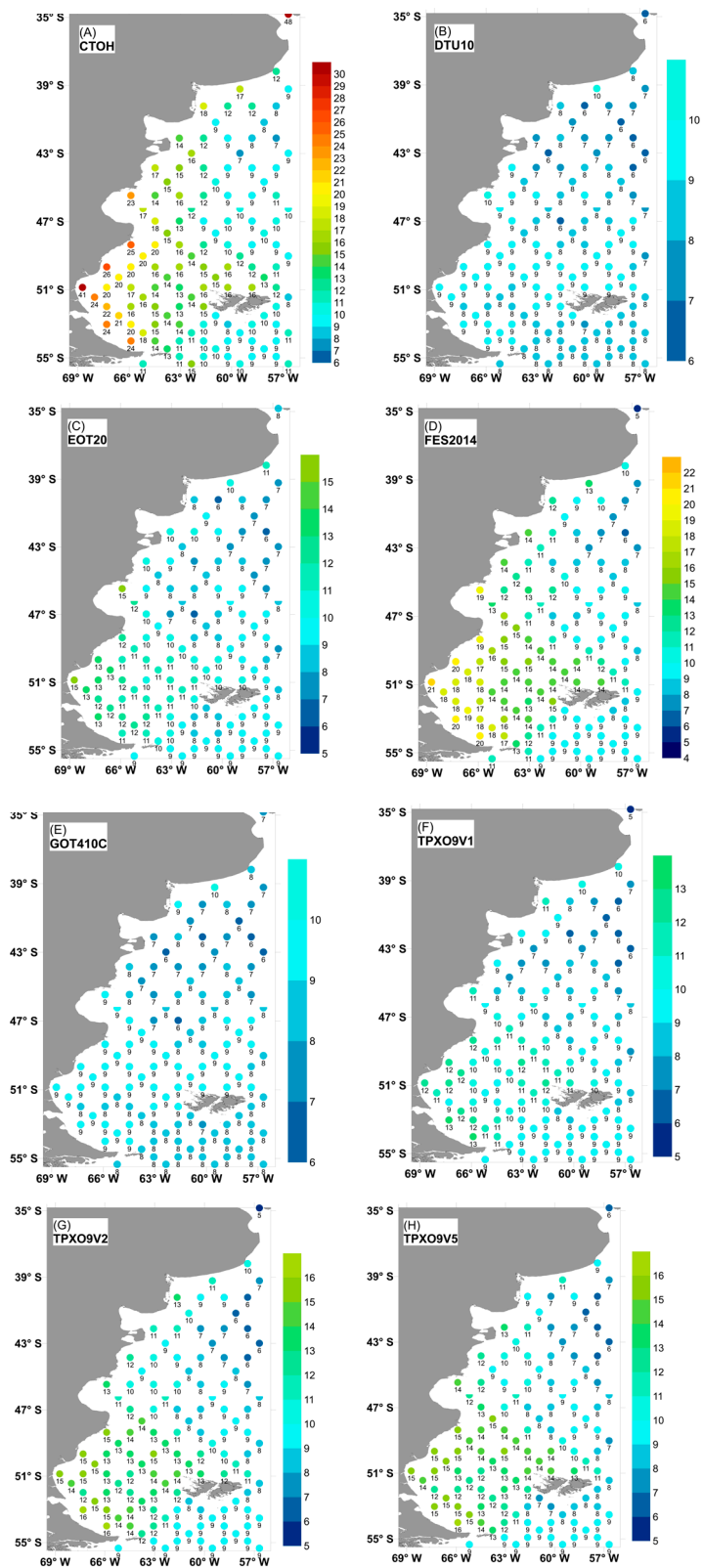


Fig. 6.
 Number of constituents with amplitudes larger than or equal to 2 cm from (A) CTOH, (B)DTU10, (C) EOT20, (D) FES2014, (E) GOT410c, (F) TPXO9v1, (G) TPXO9v2, (H)TPXO9v5.

not change with the addition of new constituents. As an example, results from the crossover that consider the highest number of constituents with amplitudes larger than or equal to 2 cm, located at 50.856°S and 68.733°W, are shown in Table 2. This cross-track belongs to a macrotidal regime area and there, both FES2014 and CTOH, minimize the VRSL values with respect to the other models by considering more constituents than them. The VRSLs taking into account only the nine common constituents at this location are very similar for all the models. These values range from 0.078 m² for FES2014 to 0.085 m² for GOT410c. Adding the remaining constituents sorted by decreasing amplitude, it is observed a progressive reduction of the VRSLs. The major reduction percentage is associated with CTOH and reaches 57.32% with respect to the value obtained with the nine main common constituents, and involves a total of 18 constituents. However, the lowest VRSL value corresponds to FES2014, with 0.034 m², and it represents a reduction of 56.41% with respect to the 9 common constituents. In this case, 23 constituents are considered in total. TPX09v2 also presents a good performance by considering 17 tide waves that yield a VRSL value of 0.044 m² and improve the original value from the 9 common constituents by 46.41%. The two models with the lowest number of constituents (DTU10 and GOT410c) have the highest VRSL values and the inability to reduce them when depleting the considered waves. This information is summarized in Table 2.

When the amplitudes and phases of the common constituents among models and CTOH are compared at the mentioned location values appear to be very similar. This is an expected behavior, considering the similarity of the VRSL values found when removing the tide using only the 9 common tide components (Table 2). Both epoch and amplitude are practically identical for all constituents of each model and CTOH. The differences in amplitudes (if any) are insignificant, of the order of a millimeter for the smaller amplitude constituents and a centimeter for those with larger amplitudes (M_2 , S_2 , N_2). And in the case of phases, the differences are of the order of a degree, except for Q_1 between CTOH and the rest of the models, where the discrepancy reaches almost 50°.

DISCUSSION

The differences found in the predictions obtained with the several models and the CTOH can be due to a variety of causes. We consider the use of different software tools, the methodology applied in the inference of waves of each algorithm, and errors in obtaining the harmonic constants (Zaron & Elipot, 2021). Thus, the discrepancies in the VRSL maps can be attributed to the better modeling of the tide by the models that have lower VRSL values and whose areas over PS, bounded by those values, are less extensive. In this case, for most of the domain, this is the situation with FES2014 and CTOH. These results suggest that the other models do not remove some of the tide variability from the residuals of sea level heights. However, the fact that the largest discrepancies in VRSL values are found in the southern part of the shelf may be attributed to the influence of bathymetry in that region. It is known that in shallow waters, accurate acquisition of tidal constituents is strongly dependent on bathymetry and the shape of the shelf (Andersen, 1999). The existence of a larger number of constituents toward the shore shown through the analysis of the number of constituents with amplitudes larger than or equal to 2 cm at each location is consistent with the shoaling that takes place in this area, and the appearance of new constituents in response to that forcing. For average shelf depths, the waves are strongly influenced by linear Kelvin wave dynamics and by basin resonances. The distortions

		<i>FES2014</i>		<i>CTOH</i>			<i>TPX09v2</i>			<i>EOT20</i>		
N. Const.	Const.	VRSL (m ²)	VRSL Red. %	Const.	VRSL (m ²)	VRSL Red. %	Const.	VRSL (m ²)	VRSL Red. %	Const.	VRSL (m ²)	VRSL Red. %
9	M ₂ , S ₂ , N ₂ , K ₂ , K ₁ , O ₁ , P ₁ , M ₄ , Q ₁	0.078	0	M ₂ , S ₂ , N ₂ , K ₂ , K ₁ , O ₁ , P ₁ , M ₄ , Q ₁	0.082	0	M ₂ , S ₂ , N ₂ , K ₂ , K ₁ , O ₁ , P ₁ , M ₄ , Q ₁	0.082	0	M ₂ , S ₂ , N ₂ , K ₂ , K ₁ , O ₁ , P ₁ , M ₄ , Q ₁	0.079	0
10	+Nu2	0.063	19.23	+2N2	0.075	8.537	+Nu2	0.067	18.39	+2N2	0.072	8.861
11	+MN4	0.062	20.51	+Nu2	0.06	26.83	+2N2	0.062	24.48	+T2	0.07	11.39
12	+2N2	0.055	29.49	+L2	0.05	39.02	+Mu2	0.059	27.65	+MM	0.07	11.39
13	+L2	0.045	42.31	+MS4	0.046	43.9	+L2	0.05	39.22	+S1	0.07	11.39
14	+Mu2	0.041	47.44	+Mu2	0.042	48.78	+MS4	0.047	43.00	+SA	0.071	10.13
15	+M6	0.043	44.87	+Lambda2	0.041	50	+MN4	0.044	46.16	+MF	0.071	10.13
16	+Lambda2	0.041	47.44	+MN4	0.037	54.88	+MF	0.044	46.41	+SSA	0.07	11.39
17	+MS4	0.037	52.56	+T2	0.035	57.32	+S1	0.044	46.41	+J1	0.07	11.39
18	+T2	0.035	55.13	+M6	0.035	57.32						
19	+J1	0.035	55.13									
20	+MNS2	0.035	55.13									
21	+S1	0.035	55.13									
22	+N4	0.034	56.41									
23	+MF	0.034	56.41									
		<i>TPX09v5</i>		<i>TPX09v1</i>			<i>DTU10</i>			<i>GOT410c</i>		
N. Const.	Const.	VRSL (m ²)	VRSL Red. %	Const.	VRSL (m ²)	VRSL Red. %	Const.	VRSL (m ²)	VRSL Red. %	Const.	VRSL (m ²)	VRSL Red. %
9	M ₂ , S ₂ , N ₂ , K ₂ , K ₁ , O ₁ , P ₁ , M ₄ , Q ₁	0.0847	0	M ₂ , S ₂ , N ₂ , K ₂ , K ₁ , O ₁ , P ₁ , M ₄ , Q ₁	0.082	0	M ₂ , S ₂ , N ₂ , K ₂ , K ₁ , O ₁ , P ₁ , M ₄ , Q ₁	0.087	0	M ₂ , S ₂ , N ₂ , K ₂ , K ₁ , O ₁ , P ₁ , M ₄ , Q ₁	0.085	0
10	+Nu2	0.0701	17.24	+2N2	0.077	6.098	S1	0.086	1.149	S1	0.085	0
11	+Mu2	0.0674	20.43	+MS4	0.073	10.98						
12	+2N2	0.0697	17.71	+MN4	0.071	13.41						
13	+L2	0.0605	28.57	+MF	0.07	14.63						
14	+MS4	0.0567	33.06	+MM	0.07	14.63						
15	+MN4	0.0539	36.36	inferred	0.0592	27.8						
16	+MF	0.0537	36.60									

Table 2. VRSL values and their corresponding percentage reduction when adding constituents in a crossover at 50.856°S and 68.733°W

of the normal harmonic variations of tidal levels can be represented by the addition of higher harmonics (Pugh & Woodworth, 2014). Therefore the better modeling of the astronomical tide obtained using CTOH and FES2014 can be attributed to the larger number of constituents they consider (73 the CTOH and 34 the FES2014) as they include several long-period and short-period constituents that the other models do not, even when considering the inference of constituents. Thus, it follows that the reduction in VRSL values is mainly due to the addition of minor constituents since it is seen that regions with the biggest discrepancy between models in the VRSL values match with those that register the largest number of constituents. In particular, the analysis of the reduction of VRSL of the crossover with the highest number of constituents, belonging to the southern region of the domain, reveals the importance of the inclusion of minor constituents to better model the tide. Usually, the larger the number of tidal stationary constituents, the better the accuracy of tidal prediction. However, the inclusion of additional unnecessary constituents does not significantly improve the accuracy of the prediction (Lee, 2004; Lee 2007). This is the case of the cross-track located in the estuary of the Río de la Plata, where CTOH counts more than 40 constituents to explain the tide, when the rest of the models do not exceed 9, and even so, lower values of VRSL are obtained from them. The same behavior is observed in the areas outside the PS (to the south and east of the domain) that are part of regions with mesoscale activity. Indeed, Haigh (2019) discuss different works achieved about tides and their non-stationary behavior related to non-astronomical forcing. Thus, it is suggested that a portion of the variance in those regions is due, probably, to the interaction of tides with mesoscale that generates new constituents susceptible to the harmonic analysis method used by CTOH.

This work allows us to state that the VRSL methodology to compare the performance between the different models and the CTOH may be superior to the traditional method through RMS over the PS, if the aim is to assess the performance considering the totality of its constituents. If, on the other hand, the goal is to compare constituents, both the RMS method and the predictions method are adequate. It was possible to verify that the correct addition of minor constituents to the major ones enhances tide modeling, obtaining a reduction in VRSL values of more than 56% in the case of CTOH and FES2014. This improvement would not have been detected by the RMS method since the nine major and common constituents of models and CTOH are practically equal in amplitude and phase.

In the areas of the open ocean domain where the tide presents micro-ranges, it is observed that the nine major and common astronomical waves model the tide satisfactorily in all cases and, proof of this are the VRSL values tending to zero for all the models and CTOH.

In summary, over the PS, the proposed method to compare tidal models by VRSL proved to be essential to choose the best fitting one. On the other hand, when setting boundary conditions or modeling the astronomical tide to understand the processes associated with it or to perform a wide range of dynamics and circulation studies, it still may not be sufficient to consider only the nine major constituents. While it is true that the principal semi-diurnal lunar constituent (M_2) explains more than 80% of the variance in the PS, the remaining variability associated with the tide, which will be no more than 20% of the total, may be significant given the very large tidal range recorded in this area. It is also observed that when using a larger number of constituents than the common ones, the VRSL drops tending to zero. Therefore, the astronomical tide could be significantly underestimated if these minor constituents are not considered, since there is variability associated with the tide that is not represented.

Finally, it is important to highlight, although it is well known, that as long satellite height series are available all over the globe, the comparison of tidal models through VRSL could be replicated for any region of the ocean.

ACKNOWLEDGEMENTS

This work was supported by the project PIDDEF 10/20, Ministerio de Defensa and the project B-ESCM-0010/20, Escuela de Ciencias del Mar, Universidad de La Defensa Nacional.

REFERENCED LITERATURE

- Andersen, O.B. (1999). Shallow water tides in the Northwest European shelf region from TOPEX/POSEIDON altimetry. *Journal of Geophysical Research*, *104*, 7729–7741. <https://doi.org/10.1029/1998JC900112>.
- Bhagawati, C., Pandey, S., Dandapat, S., & Chakraborty, A. (2018). Dynamical significance of tides over the Bay of Bengal. *Dynamics of Atmospheres and Oceans*, *82*, 89–106. <https://doi.org/10.1016/j.dynatmoce.2018.05.002>.
- Birol, F., Fuller, N., Lyard, F., Cancet, M., Niño, F., Delebecque, & C., Fleury S. (2017). Coastal Applications from Nadir Altimetry: Example of the X-TRACK Regional Products. *Advances in Space Research*, *59*, 936–953. <https://doi.org/10.1016/j.asr.2016.11.005>.
- Byun D.S. & Hart D.E. (2019). On robust multi-year tidal prediction using T_Tide. *Ocean Science Journal*, *54*, 657–671. doi.org/10.1007/s12601-019-0036-4.
- Carrère, L., Faugère, Y. & Ablain, M. (2016). Major improvement of altimetry sea level estimations using pressure-derived corrections based on ERA-Interim atmospheric reanalysis. *Ocean Science*, *12*, 825–842. doi.org/10.5194/os-12-825-2016.
- Cartwright, D.E. (1985). Tidal prediction and modern time scales. *International Hydrographic Review*. LXII (1), 127–138.
- Chelton, D.B., Ries, J.C., Haines, B.J., Fu, L.-L., Callahan, P.S. (2001). Satellite Altimetry. In: Fu, L.-L. and Cazenave, A. (Eds), *Satellite Altimetry and Earth Sciences: A Handbook of Techniques and Applications*. *International Geophysics Series* (pp 1–131), Volume 69, Academic Press, San Diego, California, USA.
- D’Onofrio, E.E., Oreiro, F.A., Grismeyer, W.H., Fiore, M.M. E. (2016). Predicciones precisas de marea astronómica calculadas a partir de altimetría satelital y observaciones costeras para la zona de Isla Grande de Tierra del Fuego, Islas de los Estados y Canal de Beagle. *GEOACTA* *40*(2), 60–75. <http://ppct.caicyt.gov.ar/index.php/geoacta/article/view/5354>
- de Azkue, M.F. (2017). *Caracterización de la marea en el Atlántico Sudoccidental utilizando datos de altimetría satelital y su comparación con soluciones de modelación numérica*. Tesis de Licenciatura. Buenos Aires, Argentina: Departamento de Ciencias de la Atmósfera y los Océanos, Facultad de Ciencias Exactas y Naturales, Universidad de Buenos Aires.
- de Azkue, M.F., D’Onofrio, E.E., & Banegas, L. (2021). Development of an empirical chart datum model for a region of the Southwest Atlantic Ocean. *Ocean and Coastal Research*, *69*, 1–11, <https://doi.org/10.1590/2675-2824069.21-028mfd>.
- Desai, S. D. & Ray, R. D. (2014). Consideration of tidal variations in the geocenter on satellite altimeter observations of ocean tides. *Geophysical Research Letters*, *41*, 2454–2459, <https://doi.org/10.1002/2014GL059614>
- Desportes, E., Obligis, E., & Eymard, L. (2007). On the wet tropospheric correction for altimetry in coastal regions. *IEEE Trans Geoscience and Remote Sensing*, *45*(7), 2139–2142, <https://doi.org/10.1109/TGRS.2006.888967>.
- Egbert, G. D. & Ray, R. D. (2001). Estimates of M2 tidal energy dissipation from TOPEX/Poseidon altimeter data. *Journal of Geophysical Research Oceans*, *106*(C10), 22475–22502, <https://doi.org/10.1029/2000jc000699>.
- Egbert, G.D. & Erofeeva, S.Y. (2002). Efficient inverse modeling of barotropic ocean tides. *Journal of Atmospheric and Oceanic Technology*, *19*, 183–204, [https://doi.org/10.1175/1520-5940426\(2002\)019](https://doi.org/10.1175/1520-5940426(2002)019).

- Erofeeva, S., Padman, L., & Howard, L. (2020). Tide Model Driver (TMD) version 2.5, Toolbox for Matlab (https://www.github.com/EarthAndSpaceResearch/TMD_Matlab_Toolbox_v2.5), GitHub. Retrieved [10-07-2022].
- Glorioso P.D. (2000). Patagonian shelf 3D tide and surge model. *Journal of Marine Systems*, *24*, 141–151.
- Glorioso, P.D. & Flather, R.A. (1998). The Patagonian Shelf tides. *Progress in Oceanography*, *40*, 1-4: 263-283, [https://doi.org/10.1016/S0079-6611\(98\)00004-4](https://doi.org/10.1016/S0079-6611(98)00004-4).
- Glorioso, P.D. & Simpson, J.H. (1994). Numerical modelling of the M2 tide on the northern Patagonian Shelf. *Continental Shelf Research*, *14*, 267-278, [https://doi.org/10.1016/0278-4343\(94\)90016-7](https://doi.org/10.1016/0278-4343(94)90016-7).
- Green, J. A. M., Green, C. L., Bigg, G. R., Rippeth, T. P., Scourse, J. D., & Uehara, K. (2009). Tidal mixing and the meridional overturning circulation from the Last Glacial Maximum. *Geophysical Research Letters*, *36*, L15603.
- Haigh, I.D., Pickering, M.D., Green, J.A.M., Arbic, B.K., Arns, A., Dangendorf, S., Hill, D., Horsburgh, K., Howard, T., Idrer, D., Jay, D.A., Janicke, L., Lee, S.B., Muller, M., Schindelegger, M., Talke, S.A., Wilmes, S.B., & Woodworth, P.L. (2019). The Tides They Are a-Changin: A comprehensive review of past and future nonastronomical changes in tides, their driving mechanisms and future implications. *Reviews of Geophysics*, *58*(1), <https://doi.org/10.1029/2018RG000636>.
- Hart-Davis, M.G., Piccioni, G., Dettmering, D., Schwatke, C., Passaro, & M., Seitz, F. (2021a). EOT20: a global ocean tide model from multi-mission satellite altimetry. *Earth System Science Data*, *13*, <https://doi.org/10.5194/essd-13-3869-2021>.
- Hart-Davis, M.G., Dettmering, D., Sulzbach, R., Thomas, M., Schwatke, y C., Seitz, F. (2021b). Regional Evaluation of Minor Tidal Constituents for Improved Estimation of Ocean Tides. *Remote Sensing in Earth Systems Sciences*, *13*, 3310, <https://doi.org/10.3390/rs13163310>.
- Holgate S.J., Matthews, A., Woodworth, P.L., Rickards, L.J., Tamisiea, M.E., Bradshaw, E., Foden P.R., Gordon, K.M., Jevrejeva, S. & Pugh, J. (2013). New data systems and products at the Permanent Service for Mean Sea Level. *Journal of Coastal Research*, *29*(3), 493–504.
- Kang, D. (2012). Barotropic and Baroclinic Tidal Energy. In: A. Z. Ahmed (Ed.), *Energy Conservation*, (pp 57-72). INTECH, London, United Kingdom, <https://doi.org/10.5772/52293>.
- Koop, R. & Rummel, R. The Future of Satellite Gravimetry. Report from the *Workshop on The Future of Satellite Gravimetry*. 12-13 April 2007, ESTEC, Noordwijk, The Netherlands.
- Lee, T.-L. (2004). Back-propagation neural network for long-term tidal predictions. *Ocean Engineering*, *31*(2), 225–238, [https://doi.org/10.1016/s0029-8018\(03\)00115-x](https://doi.org/10.1016/s0029-8018(03)00115-x).
- Lee, T.L., Makarynsky, O., Shao C.C. (2007). A Combined Harmonic Analysis–Artificial Neural Network Methodology for Tidal Predictions. *Journal of Coastal Research*, *233*, 764-770, <https://doi.org/10.2112/05-62204921>.
- Lyard, F., Lefevre, T., Francis, O. (2006). Modelling the global ocean tides: Modern insights from FE52004. *Ocean Dynamics*, *56*, 394–415, <https://doi.org/10.1007/s10236-006-0086-x>.
- Matte, P., Jay, D.A., & Zaron, E.D. (2013). Adaptation of Classical Tidal Harmonic Analysis to Nonstationary Tides with Application to River Tides. *Journal of Atmospheric and Oceanic Technology*, *569*-589, <https://doi.org/10.1175/JTECH-D-12-00016.1>.
- Middleton, J.H. & Bode, L. (1987). Poincaré waves obliquely incident to a continental shelf. *Continental Shelf Research*, *7*, 177-190.
- Moreira D., Simionato, C.G., & Dragani, W (2011). Modeling ocean tides and their energetics in the North Patagonia Gulfs of Argentina. *Journal of Coastal Research*, *27*(1), 87–102.
- Munk, W.H. y Cartwright, D.E. (1966). Tidal spectroscopy and prediction. *The Royal Society Publishing*. <https://doi.org/10.1098/rsta.1966.0024>.
- Oreiro, F.A., D'Onofrio, E.E., Grismeyer, W.H., Fiore, M.E.E., & Saraceno, M. (2014). Comparison of tide model outputs for the northern region of the Antarctic Peninsula using satellite altimeters and tide gauge data. *Polar Science*, *8* (1), 10-23. <https://doi.org/10.1016/j.polar.2013.12.001>.
- Palma, E.D., Matano, R.P., & Piola, A.R. (2004). A numerical study of the Southwestern Atlantic Shelf circulation: Barotropic response to tidal and wind forcing. *Journal of Geophysical Research*, *109*, C08014. <https://doi.org/10.1029/2004JC002315>.

- Palma, E.D., Matano, R. P., Tonini, M.H., Martos, P., & Combes, V. (2018). *Modelado de la dinámica oceánica en el Golfo San Jorge*. X Jornadas Nacionales de Ciencias del Mar. FCEyN –UBA –Buenos Aires. Libro de resúmenes. <http://jornadasdelmar2018.exactas.uba.ar/libro-de-resumenes-2/> p 49.
- Pugh, D. & Woodworth, P. (2014). *Sea Level Science- Understanding tides, surges, tsunamis and mean sea level*. Cambridge University Press.
- Pujol, M.I., Dibarboure, G., Le Traon, P.Y., y Klein, P. (2012). Using High-Resolution Altimetry to Observe Mesoscale Signals. *Journal of Atmospheric and Oceanic Technology*, 29(9), 1409–1416, <https://doi.org/10.1175/jtech-d-12-00032.1>
- Ray, R.D. (1999). *A Global Ocean Tide Model from TOPEX/POSEIDON Altimetry: GOT99.2*. Report available from the NASA Center for AeroSpace Information, 7121 Standard Drive, Hanover, MD 21076-1320. (301) 621-0390.
- Simionato, C.G., Dragani, W., Núñez, M., y Engel, N. (2004). A Set of 3-D Nested Models for Tidal Propagation from the Argentinean Continental Shelf to the Rio de la Plata Estuary—Part I. M2. *Journal of Coastal Research*, 893–912.
- Stammer, D., Ray, R. D., Andersen, O. B., Arbic, B. K., Bosch, W., Carrère, L., Cheng, Y., Chinn, D. S., Dushaw, B. D., Egbert, G. D., Erofeeva, S. Y., Fok, H. S., Green, J. A. M., Griffiths, S., King, M. A., Lapin, V., Lemoine, F. G., Luthcke, S. B., Lyard, F., Morison, J., Müller, M., Padman, L., Richman, J. G., Shriver, J. F., Shum, C. K., Taguchi, E., & Yi, Y. (2014). Accuracy assessment of global barotropic ocean tide models. *Review of Geophysics*, 52, 243–282, <https://doi.org/10.1002/2014RG000450>.
- Wunsch, C. & Ferrari, R. (2004). Vertical Mixing, Energy, and the General Circulation of the Oceans. *Annual Review of Fluid Mechanics*, 36(1), 281–314, <https://doi.org/10.1146/annurev.fluid.36.050802.122121>.
- Yongcun Ch. & Ole B. A. (2010). Improvement in global ocean tide model in shallow water regions. *Altimetry for Oceans and Hydrology OST-ST Meeting*. Poster, SV.1-68 45. <http://www.aviso.oceanobs.com/fileadmin/documents/OSTST/2010/ChengYongcun.pdf>
- Zaron, E.D. & Elipot S. (2021). An Assessment of Global Ocean Barotropic Tide Models Using Geodetic Mission Altimetry and Surface Drifters. *Journal of Physical Oceanography*, 51, 63–82, <https://doi.org/10.1175/JPO-D-20-0089.s1>

Apéndice: Afiliación declara por cada uno de los autores

Número afiliación	Nombre de la institución y/o organización Afiliación
1	Departamento Oceanografía, Servicio de Hidrografía Naval (SHN). Av. Montes de Oca 2124 - (C1270ABV) - Ciudad Autónoma de Buenos Aires - Argentina ✉ maria.azkue@defensa.gov.ar
2	Escuela de Ciencias del Mar, Facultad de la Armada, Universidad de La Defensa Nacional. Av. Antártida Argentina 425 - (C1104AAD)- Ciudad Autónoma de Buenos Aires - Argentina.
3	Facultad de Ingeniería, Universidad de Buenos Aires. Av. Paseo Colón 850 - (C1063ACV) Ciudad Autónoma de Buenos Aires - Argentina.
4	Facultad de Ciencias Exactas, Universidad Nacional de La Plata. Ex Calle 50 y 115, La Plata - (1900) - Buenos Aires - Argentina.

Autor	Afiliación
M.A. de Azkue	1, 2
E.E. D'Onofrio	3
A. Jacobs	4